AIChE

Temperature Profile in a Reverse Flow Reactor for Catalytic Partial Oxidation of Methane by Fast IR Imaging

M. Simeone and L. Salemme
Dipartimento di Ingegneria Chimica, Università Degli Studi di Napoli Federico II, P.le V. Tecchio, 80 - 80125 Napoli, Italy

C. Allouis
Istituto Sulle Ricerche Sulla Combustione - CNR, P.le V. Tecchio 80 - 80125, Napoli, Italy

G. Volpicelli
Dipartimento di Ingegneria Chimica, Università Degli Studi di Napoli Federico II, P.le V. Tecchio, 80 - 80125 Napoli, Italy

DOI 10.1002/aic.11565
Published online September 4, 2008 in Wiley InterScience (www.interscience.wiley.com).

Catalytic partial oxidation of methane with air was investigated in a reverse flow reactor with commercial Rh/Al_2O_3 catalyst in pellets. Temperature profile of the catalyst bed was measured by fast IR thermography and product composition was measured with a continuous gas analyzer. The effect of internal heat recovery on reactor performance and catalyst thermal stress is presented and compared with steady state operation. Feed direction switching time, total flow rate, and methane to oxygen ratio were investigated as process operating parameters. Data of catalyst bed temperature evolution during the flow cycle are presented and discussed. Comparison of dynamic heat integration with external feed preheating in terms of product composition and catalyst temperature profile is also presented. © 2008 American Institute of Chemical Engineers *AIChE J,* 54: 2689–2698, 2008
Keywords: reverse flow reactor, catalytic partial oxidation, thermography, hydrogen, internal heat recovery

Introduction

Catalytic partial oxidation of methane (CPOM) is a promising process for syngas production, achieved by feeding a substoichiometric mixture of methane and oxygen.[1–9]

The catalytic and exothermic nature of CPOM are two important aspects that favor a compact reactor design, suitable for small scale syngas production and could be used as a first reaction step for decentralized hydrogen generation. Indeed, because of the fast catalytic reaction rates, a small residence time is sufficient to reach high conversions and the heat of reaction provides the energy necessary to reach favorable reaction temperatures without external heating.

Initial investigation by Hickman and Schmidt[10] showed that reactants preheating leads to an increase in reactor temperature, with a positive effect on syngas yield. Reactors with internal heat recovery are an economic and compact way to realize feed preheating, particularly attractive for small scale syngas production plants. In 1999, Friedle and Veser[11] investigated CPOM in a multifunctional reactor with integrated counter current heat exchange between the hot effluent gases and the cold feed. They showed how internal heat exchange leads to an increase in syngas selectivity and methane conversion.[11,12] As reported by Boreskov and

Correspondence concerning this article should be addressed to M. Simeone at simeone@unina.it.

Matros, 1983,[13] an even more efficient heat integration can be achieved with a Reverse Flow Reactor (RFR),[13,14] where periodic switching of feed flow direction through the reactor realizes an internal heat exchange between the hot effluent gases and the cold feed, using the reactor itself as an energy reservoir.

The basic principle of the RFR was first illustrated by Eigenberger for incineration of waste gases[15,16] and, more recently, for the catalytic dehydrogenation of ethyl benzene.[17]

Numerical simulations[18–20] have shown that, when a RFR is used for CPOM with oxygen, unacceptably high maximum temperatures develop in the catalyst bed. Indeed, the internal heat recovery preheats the feed and increases the temperature of an adiabatic reactor way above the values reached in steady state conditions.[5] The use of air, instead of oxygen, is a possible root to reduce reactor temperature. The first experimental investigation of CPOM with air was conducted by Blanks et al., in 1990, on a pilot plant RFR.[21]

A detailed study of CPOM with air in a RFR on different alumina foam monolith catalysts was presented by Neumann et al.[22–24] They investigated RFR behavior by measuring product composition via mass spectrometry and gas chromatography and catalyst entrance and exit temperature with a thermocouple. Their extensive studies address the effect of several reactor design and operating parameters on different catalysts. The main conclusion is that RFR operation leads to a substantially increased catalyst entrance temperature compared with conventional steady state reactor operation. The increased catalyst entrance temperature efficiently reduces total oxidation of methane and results in a pronounced increase in syngas yield. Because of the increased catalyst entrance temperature, higher reactor temperatures are expected when the reactor is operated in reverse flow mode, and it becomes important, in relation to catalyst lifetime, to measure accurately the temperature reached throughout the catalyst bed.

In this work, we present the first systematic investigation of catalyst temperature profile and its periodic evolution during CPOM with air in a RFR.

The effect on catalyst temperature profile and product composition of switching time, feed flow rate, and methane to oxygen ratio is presented and compared with steady state operation.

Experimental Apparatus

The experimental apparatus, schematically reported in Figure 1, essentially consists of a quartz tube with a catalyst section length of 20 mm placed between two inert alumina spheres sections, (60 mm each). The reactor is embedded in a ceramic insulating material and is inserted in a tubular oven with a heating length of 500 mm.

The gaseous reactants, coming from pressurized vessels, are fed to the reactor by Thermal Mass Flow Controllers (Brooks 5850). Switching of flow direction through the quartz tube is achieved by means of four electrovalves synchronized in pairs and positioned as indicated in Figure 1. Throughout the text, we will name the switching period as "τ" and we will refer to a direct semiperiod, when the feed flows through the reactor from left to right and to a reverse

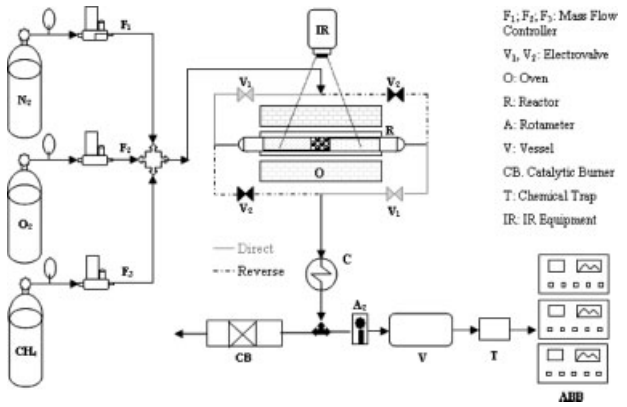

Figure 1. Experimental apparatus.

semiperiod, when the feed flows from right to left (see Figure 1).

Reactor pressure is measured with Piezo Pressure Transmitters placed immediately before and after the quartz reactor. Pressure drop in the reactor proved to be negligible.

Product composition was measured by means of an ABB Gas Analyzer, equipped with thermal conductivity sensor Caldos 17, for H_2, infrared sensor Uras 14, for CO, CO_2, and CH_4 and paramagnetic sensor Magnos 106 for O_2. After the reactor, the product stream passes through a water cooled condenser to avoid condensation in the downstream tubes. After the condenser, 0.8 Nl/min are convoyed toward the ABB analyzer, whereas the rest of the product gas is oxidized in a catalytic burner. A $CaCl_2$ trap was placed before the ABB Gas Analyzer to further reduce water content below the limits mandatory for the instrument.

Given the nonstationary nature of the reactor, a 5 l vessel was placed before the ABB Analyzer, as indicated in Figure 1, to ensured appropriate mixing of the output gas. Because of the limited volume of the vessel, this solution proved to be satisfactory up to τ ca. 350 s. For τ larger than 350 s, product composition was obtained by averaging the ABB measurements of several cycles.

Temperature profile in the catalyst bed was measured with a fast IR thermography equipment (Phoenix, Flir Systems) capable of collecting the radiation emitted in the wavelength range 2–5 μm, with a resolution of 320 $\times$ 256 pixels and an acquisition frequency of 120 Hz.

IR image acquisition was performed by following two different protocols: a continuous protocol and a discontinuous one. In the continuous protocol, the oven was kept open throughout the measurement and the reactor was operated without the ceramic insulating material. This protocol allows to measure the temperature profile evolution with great time resolution (120 frames per second); however, the absolute temperature values are affected by heat exchange between the reactor and the environment (typical temperature losses due to heat exchange are in the range 50–100°C).

In the discontinuous protocol, the IR image was acquired by rapidly opening the oven and sliding upward the ceramic insulating material to visualize the catalyst bed. The entire procedure lasted less than 5 s. To follow temperature profile throughout the period, without affecting reactor behavior

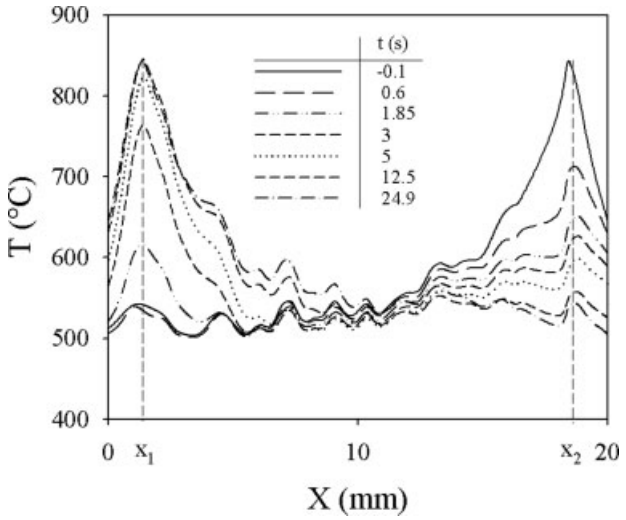

Figure 2. Catalyst bed axial temperature profile during direct semiperiod.

Reaction conditions: $CH_4/O_2 = 1.8$; total flow rate $Q = 4$ Nl/min; $\tau = 50$ s.

with repetitive acquisitions, two periods were allowed between consecutive acquisitions.

This protocol minimizes heat exchange between the reactor and the environment, thus providing a more accurate measurement of the absolute temperature values, but is limited with respect to time resolution.

The continuous protocol was used to acquire the data reported in Figures 2 and 3. The discontinuous protocol was used to acquire the data reported in Figures 4–14.

To convert IR data from photon emission to temperature, a calibration was performed by stepwise increasing oven temperature, as reported in Simeone et al., 2008.[25] The IR images were processed to gather quantitative data of temperature profile with the software ThermaCam RView. To reduce data dispersion, the temperature profiles were always

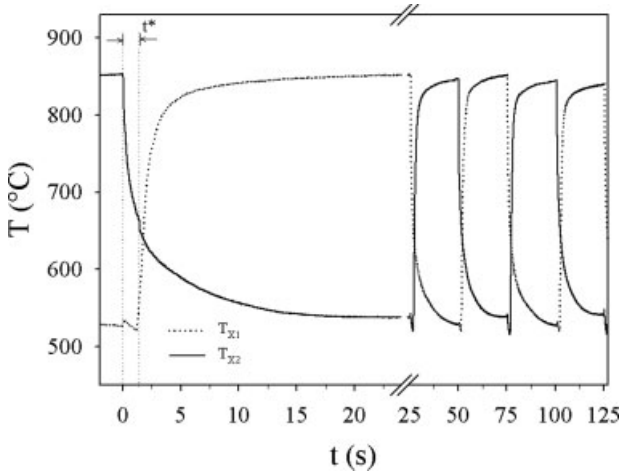

Figure 3. Temperature evolution in correspondence to x_1 and x_2 as a function of time.

Reaction conditions: $CH_4/O_2 = 1.8$; total flow rate $Q = 4$ Nl/min; $\tau = 50$ s.

Table 1. Catalyst Properties

Composition (wt%)	
Rh	0.4
Al_2O_3	Balance
Physical properties	
Bulk density (g/cm^3)	0.8
Total surface area (m^2/g)	10
Size of the spheres (mm)	2.4

calculated by averaging temperature profiles measured in correspondence of six different radial positions.

A homemade software, written in Labview, was used to control the electrovalves and the mass flow controllers, and to acquire data of temperature, pressure, and composition. When needed, the analogical signals were digitized by a National Instruments board.

The catalyst, Rh/Al_2O_3, was purchased from Engelhard (code 4406), and was supplied in 2.4 mm diameter pellets. The pellets were crushed and particles with diameter in the range $1 \div 1.18$ mm were separated and used as catalyst. To reach the desired catalyst bed length (20 mm), 5 g of catalyst were loaded in the reactor. Catalyst physical properties are reported in Table 1 (data provided by the supplier). Spheres of α-Al_2O_3, with diameter of 1 mm, were used as to create two inert sections before and after the catalyst bed.

Immediately after loading, the catalyst was reduced according to the following procedure: the catalyst bed was brought to 400°C in N_2 atmosphere, then while fluxing a stream of H_2 (30%) in N_2, the temperature was raised to 600°C with a 5°C/min ramp and kept at 600° for 1 h.

After the reduction step, oven temperature was brought to the desired value (180°C), however, to avoid coke formation at low temperature, the catalyst bed was heated up to ca. 700°C by oxidizing a stream of H_2 before feeding the reactants.

Results

Figure 2 reports the temperature profile in the catalyst bed as measured by continuous IR imaging, for the case of $\tau = 50$ s and considering $t = 0$ as the onset of the direct semiperiod.

For $t = -0.1$ s, that is, immediately before flow inversion, catalyst temperature shows a sharp maximum at the right hand side of the catalyst bed, where most of the oxidation takes place (upstream part of the catalyst bed) and a lower value at the left hand side of the catalyst bed, due to the endothermic reforming reactions (downstream part of the catalyst bed). This is in line with the data reported in the literature[1,2,6,26,27] for catalytic partial oxidation in steady state conditions.

As flow feed direction is inverted, the temperature progressively decreases at the right hand side of the catalyst bed and increases at the left hand side, the positions of the temperature peaks, x_1 and x_2, respectively, remaining constant with time. Because of reactor symmetry, temperature profile for $t = -0.1$ s (end of reverse semiperiod) and for $t = 24.9$ s (end of direct semiperiod) are mirror images.

A detailed analysis of temperature evolution is presented in Figure 3, where temperature in correspondence to x_1 and x_2 is reported as a function of time. Two different scales

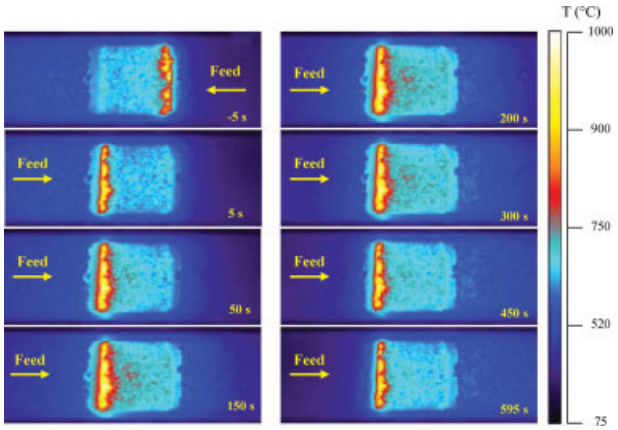

Figure 4. Reactor IR image during direct semiperiod; t = 0 is the end of reverse semiperiod.

Reaction conditions: CH_4/O_2 = 1.8; total flow rate Q = 4 Nl/min; τ = 1200 s. [Color figure can be viewed in the online issue, which is available at www.interscience.wiley.com.]

were chosen for the time axis, in order to illustrate temperature evolution during one semiperiod ($0 < t < 25$) and the periodic and symmetric behavior of the reactor ($25 < t < 125$).

After flow inversion ($t = 0$), T_{X2} decreases with time, following an exponential decay, due to the abrupt shut down of the reaction. T_{X1} increases for $t > t^*$, where t^* is the time needed for the reactants to reach the catalyst bed after flow inversion. Indeed, it is only after t^* that heat of reaction is generated in correspondence to x_1. For $0 < t < t^*$, T_{X1} decreases because of heat exchange with the environment, as it is the case for T_{X2}. Both the vanishing and forming peak have a rather fast dynamics, with most of the temperature change occurring within the first 5 s.

Figures 4 and 5 report the IR images and the corresponding temperature profiles as a function of time, for τ = 1200 s. The x dimension of the IR images, acquired according to the discontinuous protocol, is 60 mm, with the catalyst bed (20 mm) positioned in the center.

For $t = -5$ s (end of the reverse semiperiod), the temperature peak is located at the right hand side of the catalyst (x_2) and inert Section 1 is warmer than inert Section 2. Indeed, throughout the reverse semiperiod, the cold feed entering into the reactor from the right hand side has lowered the temperature of inert Section 2 and the hot product stream has increased the temperature of inert Section 1. As expected in a periodic and symmetric reactor, temperature profiles for $t = -5$ s and $t = 595$ s are mirror images.

For $t = 5$ s, the temperature peak is already positioned at the left hand side of the catalyst bed, x_1, and the vanishing peak is almost completely disappeared. These fast temperature changes occurring in the catalyst bed are in agreement with the data reported in Figure 2 and are independent of inert temperature changes, which follow slower dynamics (notice that for $t = -5$ s and $t = 5$ s inert temperature profile has not changed). Further peak temperature evolution, occurring throughout the semiperiod, should be related to temperature changes in the upstream inert section. Although the maximum amount of heat accumulated in inert Section 1 has a maximum value at the point of flow reversal, temperature immediately before the catalyst bed (T_{X0}), reported in Figure 6a, reaches a maximum later on in the semiperiod, due to heat coming from the reacting zone. T_{X1} follows the same trend as T_{X0} and starts to decrease as soon as the progressive cooling of inert Section 1 causes a decrease of T_{X0}. The lag time between flow reversal and the achievement of the maximum in T_{X1} and T_{X0} is related to reactor configuration (type and quantity of inert material, catalyst, flow rate, etc.). In agreement with Veser et al.[12] catalyst bed exit temperature, T_{X3}, varies throughout the cycle less then T_{X0}. Because of the periodic and symmetric nature of the process, $T_{X3}(t = 0) = T_{X0}(t = \tau/2)$. For τ = 1200 s, T_{X3} slightly decreases immediately after flow inversion and reaches a minimum value within the first 50 s. This is due to the fast temperature drop in correspondence of x_2 (vanishing peak). After the minimum, T_{X3} increases and reaches a maximum value for t = 200 s ca. followed by a slow decrease. This is because of the increasing temperature of the upstream part of the catalyst bed, where the oxidation reactions take place. It is worth noting that T_{X3} reaches its maximum value after T_{X1}, due to the time needed for heat exchange from x_1 to x_3.

Temperature evolution as a function of time was measured also for τ = 350 s and the data are reported in Figure 6b. T_{X0} and T_{X1} follow the same trend as in the case of τ = 1200 s, for the first 175 s, when flow inversion occurs. T_{X3} reaches a minimum value shortly after flow reversal and levels off at a plateau value.

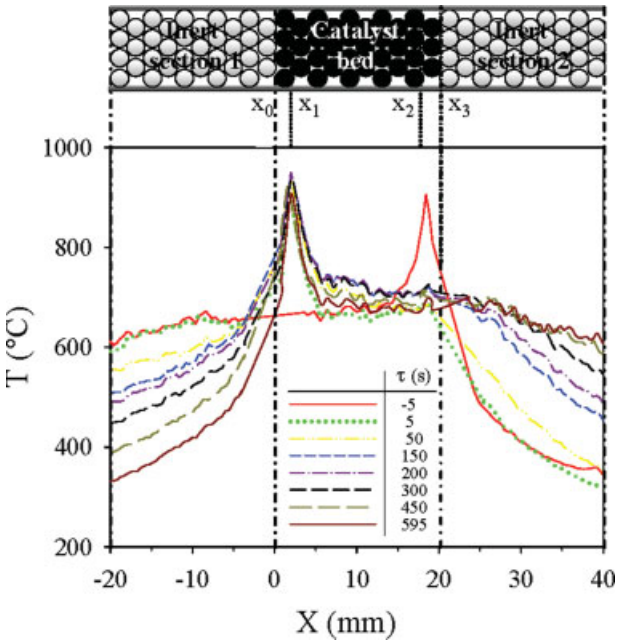

Figure 5. Reactor temperature profile during direct semiperiod; t = 0 is the end of reverse semiperiod.

Reaction conditions: CH_4/O_2 = 1.8; total flow rate Q = 4 Nl/min; τ = 1200 s. [Color figure can be viewed in the online issue, which is available at www.interscience.wiley.com.]

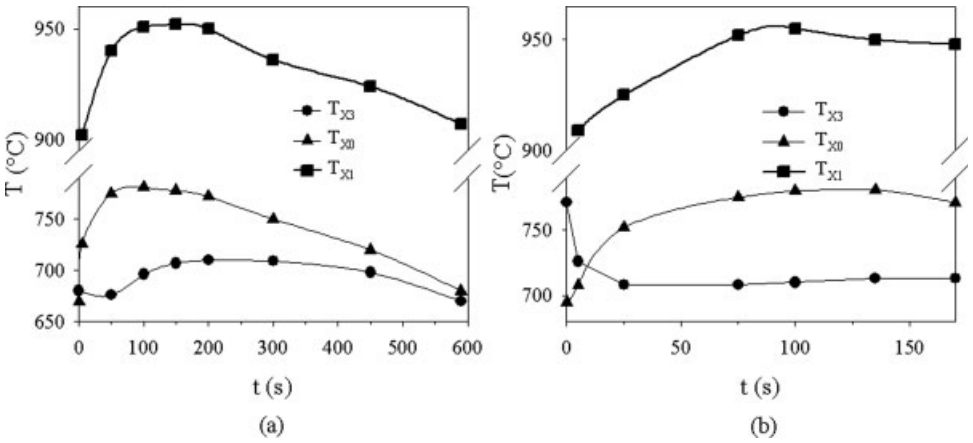

Figure 6. Temperature evolution at position x_0, x_1, and x_3 as a function of time: τ = 1200 s (a); τ = 350 s (b).

Reaction conditions: $CH_4/O_2 = 1.8$; total flow rate $Q = 4$ Nl/min.

Figures 7(a–d) reports reactor performance as a function τ in terms of methane conversion (x_{CH4}), moles of hydrogen (n_{H2}), moles of carbon monoxide (n_{CO}), and moles of syngas produced per mole of methane in the feed, respectively, calculated as follows:

$$
\begin{aligned}
x_{CH4} &= \frac{y_{CO} + y_{CO_2}}{y_{CO} + y_{CO_2} + y_{CH_4}} \\
n_{H2} &= \frac{y_{H_2}}{y_{CO} + y_{CO_2} + y_{CH_4}} \\
n_{CO} &= \frac{y_{CO}}{y_{CO} + y_{CO_2} + y_{CH_4}} \\
n_{syngas} &= \frac{y_{H2} + y_{CO}}{y_{CO} + y_{CO_2} + y_{CH_4}}
\end{aligned}
\qquad (1)
$$

where y_{CO}, y_{CO2}, y_{H2}, and y_{CH4} are components volume fractions as measured by the continuous gas analyzer. x_{CH4}, n_{H2}, n_{CO}, and n_{syngas} show a nonmonotone trend as a function of τ, with a maximum for $\tau = 350$ s. If compared with the values obtained when, in similar conditions, the reactor is operated in steady state, the improvement is as high as 14% for x_{CH4} and 21% for syngas production.

In the τ range 250–500 s, x_{CH4}, n_{H2}, n_{CO}, and n_{syngas} show a wide plateau and start to decrease for τ greater than 750 s. The loss of reactor performance indicates that dynamic heat recovery becomes less efficient as reactor behavior approaches stationary conditions ($\tau = \infty$). On the other hand, the loss of reactor performance as τ approaches zero can be ascribed to the following aspects: (a) the fraction of fresh feed lost at each flow inversion (due to reactor wash out) increases; (b) mean catalytic bed temperature decreases (see Figure 8).

Reactor temperature profile, as a function of τ, is presented in Figures 8a, b where the temperature profiles measured at the beginning ($t = 5$ s) and at the end of the semiperiod ($t = \tau/2$–5 s) are presented. For comparison, the temperature profile when the reactor is operated with no flow inversion (SS) is also reported (open circles).

Figure 8a shows that temperature in inert Section 1 is always much greater than in the steady state case. It increases with τ, up to $\tau = 350$ s and only marginal improvements are measured for higher τ, showing that no further energy can be stored in inert Section 1 by increasing the switching period over 350 s.

The temperature profiles at the end of the direct semiperiod (Figure 8b) show a continuous decrease in inert Section 1 as a function of τ. Indeed, as τ increases, more time is available for heat exchange between inert Section 1 and the fresh feed.

The progressive temperature decrease occurring in the upstream inert section causes a temperature decrease in the catalyst bed.

Optimum reactor performance is achieved when the catalyst maintains high temperature values throughout the period and is obtained by inverting flow direction as soon as the downstream energy reservoir is entirely loaded ($\tau = 350$ s).

Figures 9–12 compare reactor behavior when operated in reverse flow ($\underline{\tau} = 350$ s) and in stationary conditions as a function of feed flow rate ($Q = 1$–5 Nl/min). In particular, Figures 9a–d show how x_{CH4}, n_{H2}, n_{CO} and n_{syngas} increase as a function of flow rate. In steady state conditions, reactor performance reaches a plateau for $Q = 5$ Nl/min, this is not the case when the reactor is operated in reverse flow mode, showing that a higher productivity can be achieved when feed preheating is integrated within the reactor.

Data of methane conversion, calculated with Aspen Plus with an isothermal equilibrium reactor are superimposed to the experimental data in Figure 9a. The calculations with Aspen Plus were performed imposing, for each flow rate, the values of bed exit temperature measures experimentally. Because of time evolution of T_{X3}, which rapidly reaches a plateau value (see Figure 9b), the calculation was performed at the value of T_{X3} measured at the end of the semiperiod.

The comparison shows that methane conversion is less than what experimentally measured.

The same discrepancy was observed by Basile et al.[6] in similar conditions and was attributed to the fact that chemical equilibrium may be reached before the end of the catalyst bed, without the contribution by the last part of the catalyst bed. Heat loss to the environment may also be responsible for the discrepancy between experimental data and thermodynamic calculations, and is more evident for low flow rates,

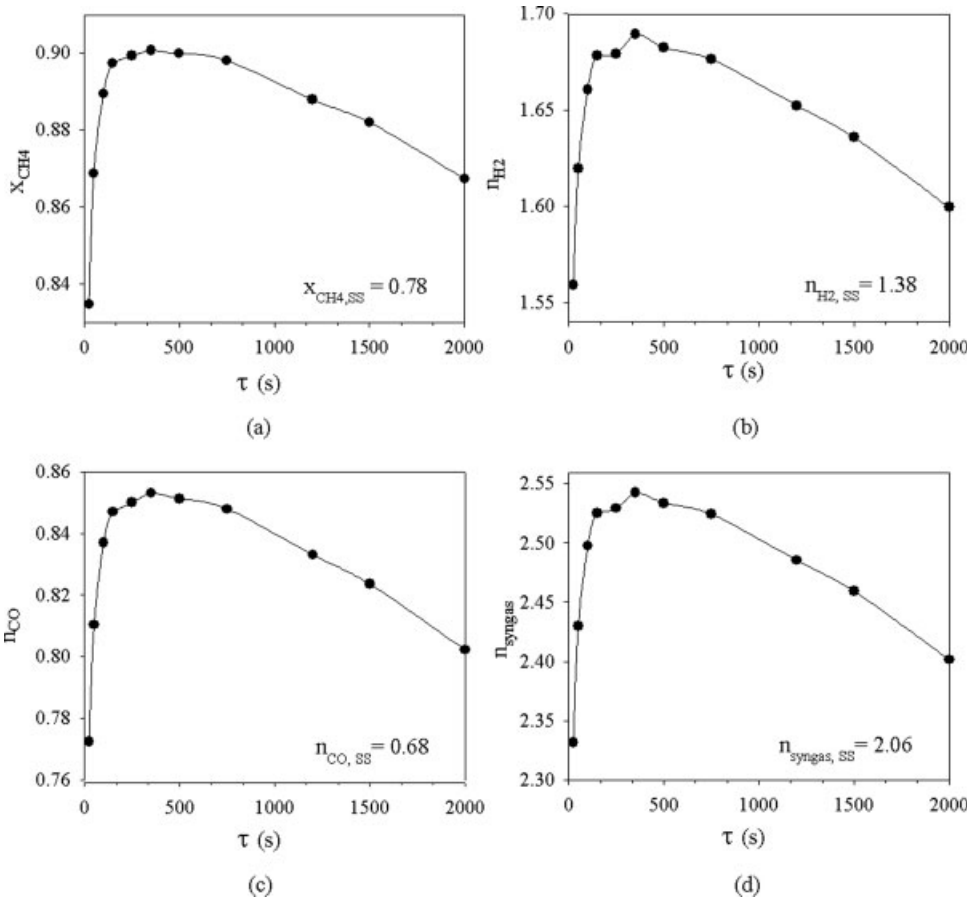

Figure 7. x_{CH4} (a), n_{H2} (b), n_{CO} (c), and n_{syngas} (d) as a function of τ. Reaction conditions: CH_4/O_2 = 1.8; total flow rate Q = 4 Nl/min.

where less heat per unit volume is generated by the reactions and the reactor is further from adiabatic conditions.

The difference in reactor performance between reverse flow and steady state case increases with flow rate. For Q = 1 Nl/min, dynamic operation does not increase significantly methane conversion and syngas production. This is in line with the data reported in Figure 10a, showing that, due to the limited amount of heat generated by the reaction, the entity of energy storage in the inert sections is modest and the temperature profiles in the catalyst bed are rather similar (compare profiles at t = 170 s and SS). As flow rate increases, a larger amount of energy is generated by the reaction, corresponding to a higher temperature of the downstream inert section. In reverse flow operation, this results in

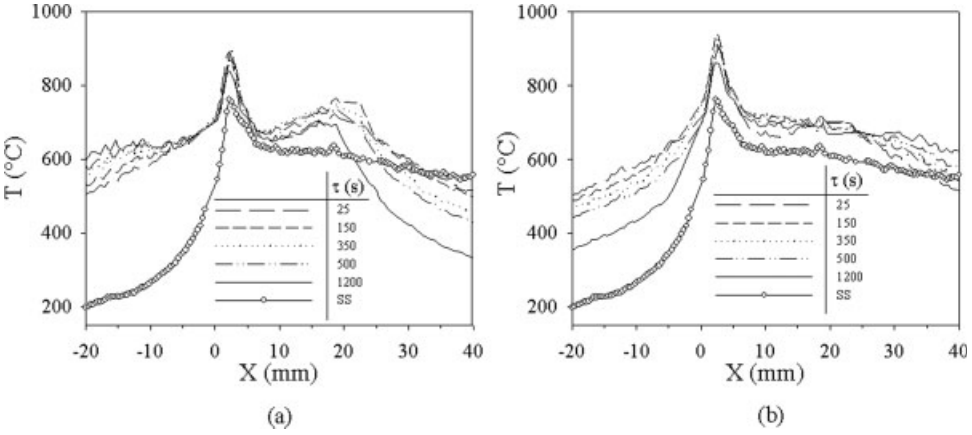

Figure 8. Reactor temperature profile as a function of τ measured at beginning (a) and at the end (b) of direct semiperiod.

Reaction conditions: CH_4/O_2 = 1.8; total flow rate Q = 4 Nl/min.

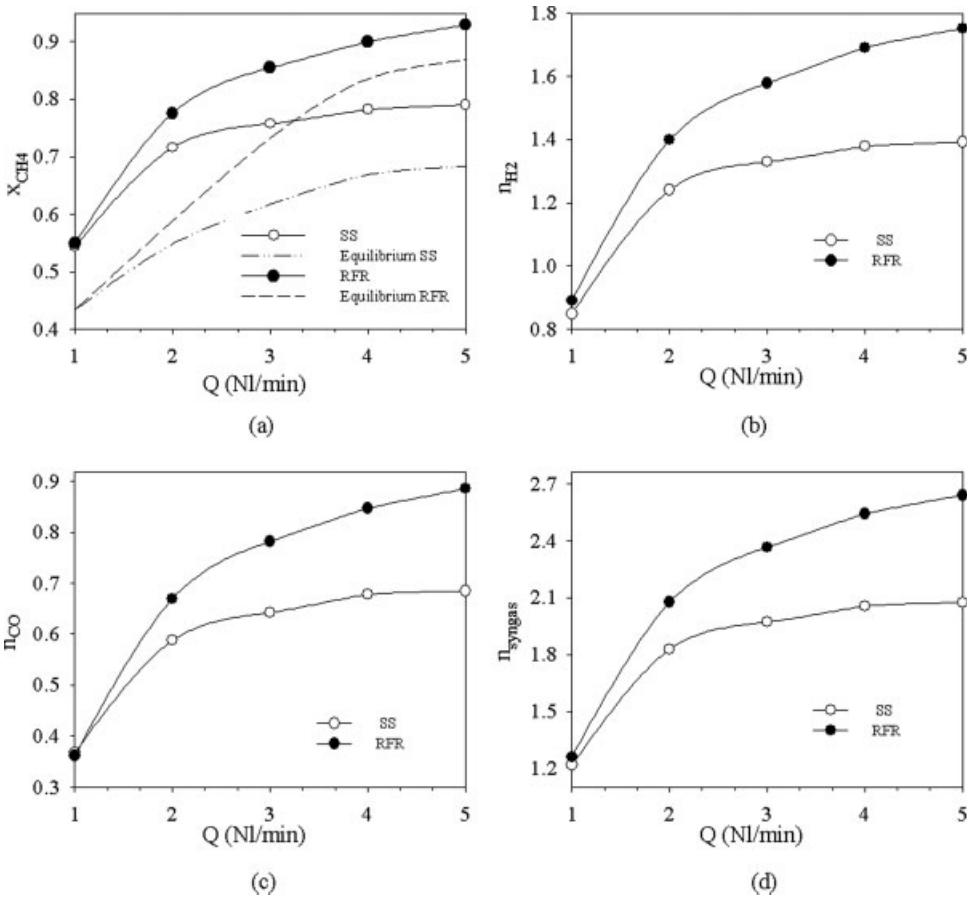

Figure 9. x_{CH4} (a), n_{H2} (b), n_{CO} (c), and n_{syngas} (d) as a function of total flow rate Q for stationary and reverse flow conditions (τ = 350 s).

Reaction conditions: $CH_4/O_2 = 1.8$.

a larger heat recovery, a higher temperature of the catalyst bed (see Figures 10b–d) and improved reactor performance with respect to steady state operation.

Figure 11 reports peak temperature (T_{X1}) as a function of flow rate for the steady state and reverse flow case. Because of dynamic heat recovery, the increment of peak temperature with flow rate in reverse flow operation is much higher than in steady state conditions.

Figures 12a, b report T_{X0} and T_{X3} as a function of feed flow rate, respectively. Because of the time evolution of T_{X0} and T_{X3}, which for $t = 350$ rapidly reach a plateau value (see Figure 6 band c), the data reported in Figure 12 refer to the value measured at the end of the semiperiod.

While in steady state operation, the increment of convective cooling with flow rate overcomes the increment of peak temperature, resulting in a decrease of T_{X0} with Q, in reverse flow conditions the same balance results in an increment of T_{X0} with Q.

As shown in Figure 12b, catalyst bed exit temperature, T_{X3}, increases with flow rate, both in steady state and reverse flow conditions. However, the temperature increment because of dynamic heat integration is higher for T_{X0} than for T_{X3}, since part of the energy recovered is converted into chemical energy, as shown by the methane conversion and syngas production data.

Figures 13a–d reports x_{CH4}, n_{H2}, n_{CO}, and n_{syngas} as a function of methane to oxygen ratio (CH_4/O_2). Methane conversion decreases with CH_4/O_2 ratio, both in steady state and in reverse flow conditions. The improvement due to the periodic switching of feed flow direction is higher at high CH_4/O_2, where methane conversion is far from unity.

The data reported in Figures 13b–d show that hydrogen and carbon monoxide production is higher in reverse flow than in steady state conditions, and that the maximum value of syngas production is achieved at higher CH_4/O_2 ratio. These results are due to the internal heat recovery realized in reverse flow conditions, which increase syngas selectivity.

To compare dynamic heat integration with external feed preheating, the reactor was operated in steady state conditions and oven temperature was varied until methane conversion reached the value obtained in reverse flow mode, with $\tau = 350$ s, that is, $x_{CH4} = 0.9$. Such a temperature resulted to be 500°C and the corresponding temperature profile, superimposed to the temperature profile in reverse flow conditions, is presented in Figure 14. Despite the differences in the upstream inert section, T_{XO} as well as the entire temperature profile throughout the catalyst bed are the same. Product composition, not shown for the sake of brevity, also proved to be identical, confirming that the RFR is equivalent to a

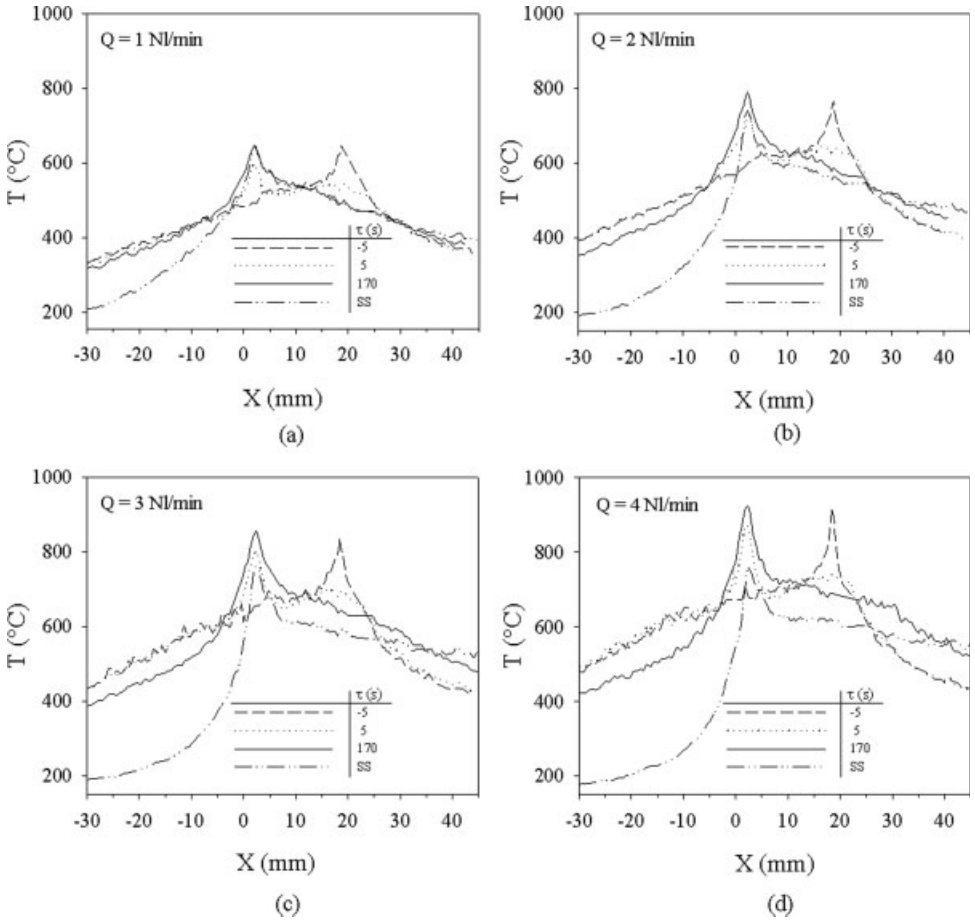

Figure 10. Reactor temperature profile for stationary and reverse flow conditions (τ = 350 s) at a different total flow rate.

(a) $Q = 1$ Nl/min; (b) $Q = 2$ Nl/min; (c) $Q = 3$ Nl/min; (d) $Q = 4$ Nl/min. Reaction conditions: $CH_4/O_2 = 1.8$.

steady state reactor with external feed preheating achieving the same T_{X0}.

Conclusions

Catalytic partial oxidation of methane with air was investigated in a reverse flow reactor with commercial rhodium catalyst as a function of switching time, total feed flow rate, and methane/oxygen ratio. A detailed analysis of catalyst temperature profile and its periodic evolution is reported, to establish the effect of internal heat recovery on catalyst thermal stress.

During dynamic reactor operation, catalyst temperature profile is determined by heat of reaction and preheating of the cold feed passing through the upstream inert section of the reactor. Fast IR imaging of the reactor revealed that most of the temperature change in the catalyst bed occurs within 5 s from flow inversion. In particular, immediately after flow inversion, temperature decreases thought the entire catalyst bed until the fresh feed reaches the catalyst, heat of reaction is generated and a new temperature peak is formed.

Further catalyst temperature evolution, occurring with slower dynamics, is related to temperature changes in the upstream inert section throughout the semiperiod. Although the maximum amount of heat accumulated in the upstream inert section has a maximum value at the point of flow reversal, the highest catalyst temperature is reached later on in the semiperiod, due to heat coming from the reacting zone.

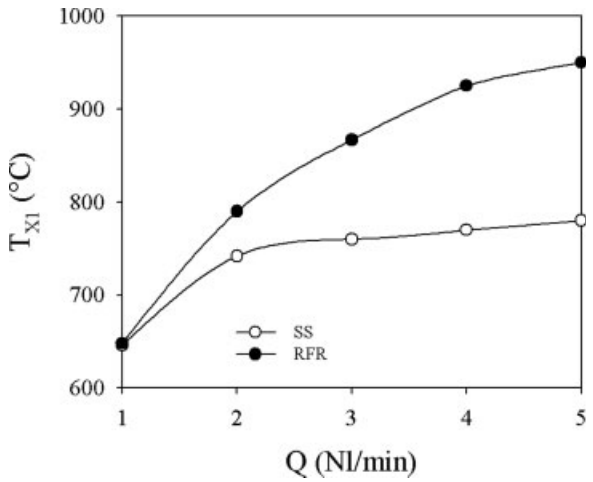

Figure 11. T_{X1} as a function of total flow rate in steady state and reverse flow mode (τ = 350 s).

Reaction conditions: $CH_4/O_2 = 1.8$.

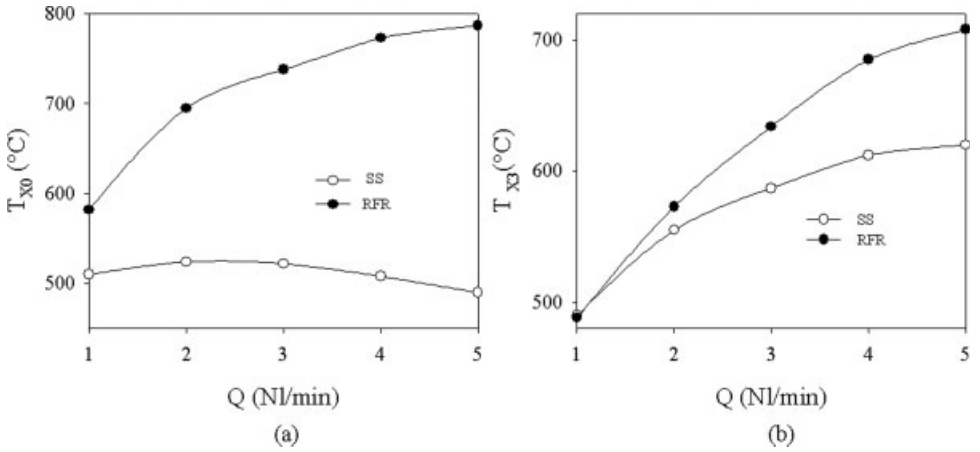

Figure 12. T_{X0} (a) and T_{X3} (b) as a function of total flow rate in steady state and reverse flow mode (τ = 350 s).

Reaction conditions: $CH_4/O_2 = 1.8$.

The effect of feed direction switching time was investigated in terms of product composition and reactor temperature profile, ant it was found that highest methane conversion and syngas production are achieved by inverting flow direction as soon as the downstream energy reservoir is entirely loaded.

Variation of feed flow rate revealed that the advantage of internal heat recovery in terms of methane conversion and syngas production increases with flow rate, due to the larger amount of heat generated and internally recovered at higher flow rates. However, while maximum catalyst temperature reaches a plateau in steady state conditions, a continuous

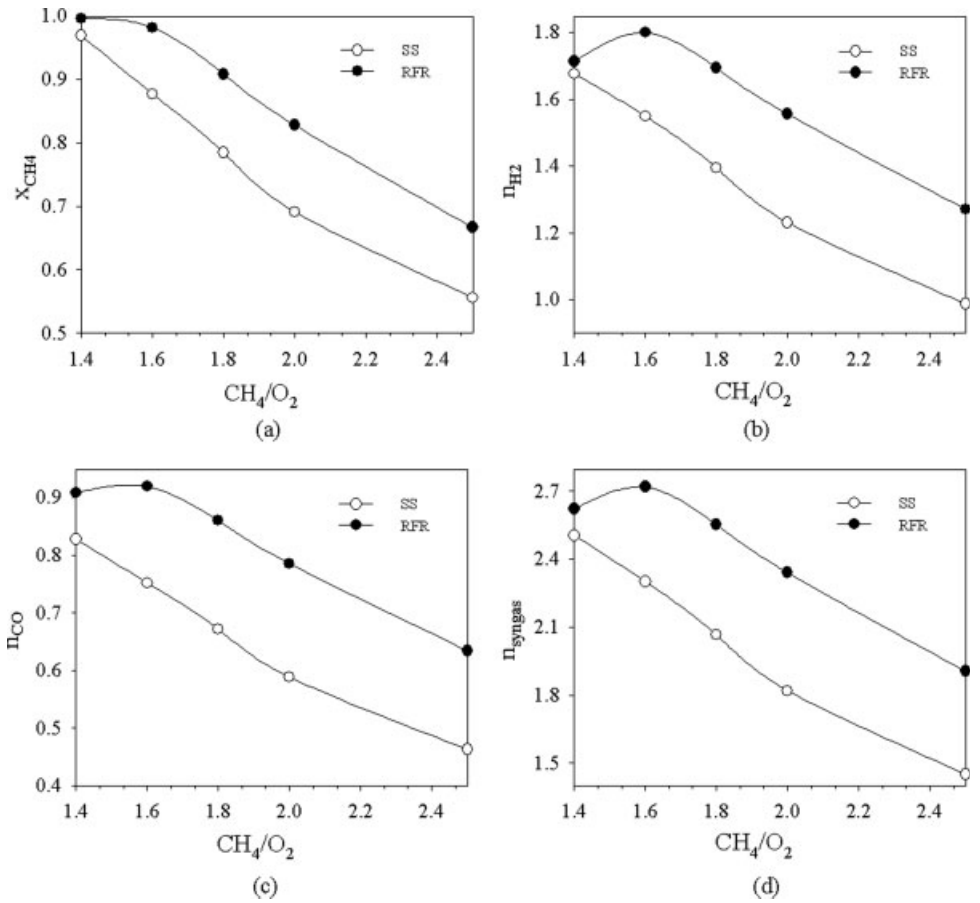

Figure 13. x_{CH4} (a), n_{H2} (b), n_{CO} (c), and n_{syngas} (d) as a function of CH_4/O_2 ratio for stationary and reverse flow conditions (τ = 350 s).

Reaction conditions: Total flow rate Q = 4 Nl/min.

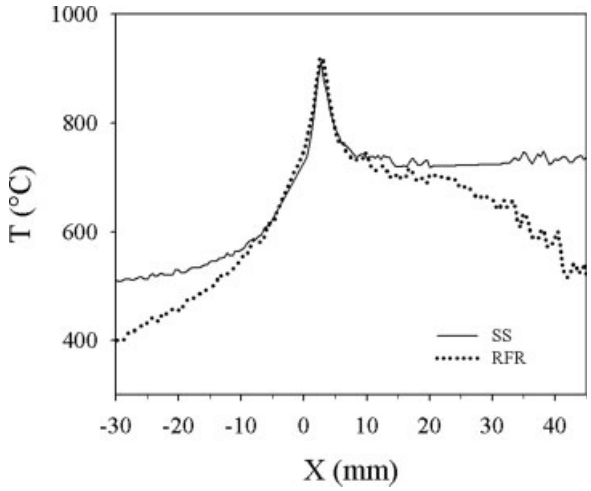

Figure 14. Reactor axial temperature profile for stationary case with external feed preheater operating at T = 500°C and reverse flow case for τ = 350 s (after 175 s from the beginning of the direct semiperiod).

Reaction conditions: $CH_4/O_2 = 1.8$, total flow rate $Q = 4$ Nl/min.

increase is present in reverse flow mode. In the flow rate range explored in this work, maximum catalyst temperature never exceeded 950°C. Further investigation is required to assess catalyst thermal stress at higher flow rates.

With respect to methane/oxygen ratio, operating the reactor in reverse flow mode, increases methane conversion and syngas production and allows to reach the maximum in syngas production with a higher methane/oxygen ratio.

Finally, dynamic heat integration was compared with external feed preheating in terms of product composition and catalyst temperature profile, and was concluded that the reverse flow reactor is equivalent to a steady state reactor with external feed preheating, achieving the same catalyst bed inlet temperature.

Acknowledgments

This work has been carried out within the framework of the project "Pure hydrogen from natural gas through reforming up to total conversion obtained by integrating chemical reaction and membrane separation" financially supported by MUR (FISR DM 17/12/2002 - year 2001).

Literature Cited

1. Bizzi M, Saracco G, Schwiedernoch R, Deutschmann O. Modeling the partial oxidation of methane in a fixed bed with detailed chemistry. *AIChE J*. 2004;50:1289–1299.
2. Tavazzi I, Maestri M, Beretta A, Groppi G, Tronconi E. Steady-state and transient analysis of a CH_4-catalytic partial oxidation reformer. *AIChE J*. 2006;52:3234–3244.
3. Schmidt LD, Bharadwaj SS. Catalytic partial oxidation of natural gas to syngas. *Fuel Process Technol*. 1995;42:109–127.
4. Ma L, Trimm D. Alternative catalyst bed configurations for the autothermic conversion of methane to hydrogen. *Appl Catal A: Gen*. 1996;136:265–273.
5. De Groote AM, Froment GF. Simulation of the catalytic partial oxidation of methane to syngas. *Appl Catal A: Gen*. 1996;138:245–264.
6. Basile F, Fornasari G, Trifirò F, Vaccari A. Partial oxidation of methane. Effect of reaction parameters and catalyst composition on the thermal profile and heat distribution. *Catal Today*. 2001;64:21–30.
7. Prettre M, Eichner C, Perrin M. The catalytic oxidation of methane to carbon monoxide and hydrogen. *Trans Faraday Soc*. 1946;42: 335b–339b.
8. Schmidt LD, Hickman DA. Steps in CH_4 Oxidation on Pt and Rh surfaces: high temperatures reactor simulations. *AIChE J*. 1993;39: 1164–1177.
9. Chan SH, Wang HM. Thermodynamic analysis of natural-gas fuel processing for fuel cell applications. *Int J Hydrogen Energy*. 2000:25;441–449.
10. Hickman DA, Schmidt LD. Production of syngas by direct catalytic oxidation of methane. *Science* 1993;259:343–346.
11. Friedle U, Veser G. Counter-current heat-exchange reactor for high temperature partial oxidation reactions. *Chem Eng Sci*. 1999;54: 1325–1332.
12. Veser G, Frauhammer J, Friedle U. Syngas formation by direct oxidation of methane. Reaction mechanisms and new reactor concepts. *Catal Today*. 2000;61:55–64.
13. Boreskov GK, Matros Y. Unsteady-state performance of heterogeneous catalytic reactions. *Catal Rev Sci Eng*. 1983;25:551–578.
14. Boreskov GK, Matros Y. Flow reversal of reaction mixture in a fixed catalyst bed. A way to increase the efficiency of chemical processes. *Appl Catal*. 1983;5:337–343.
15. Eigenberger G, Nieken U. Catalytic combustion with periodic flow reversal. *Chem Eng Sci*. 1988;43:2109–2115.
16. Nieken U, Kolios G, Eigenberger G. Fixed bed reactors with periodic flow reversal: Experimental results for catalytic combustion. *Catal Today*. 1994;20:335–350.
17. Kolios G, Eigenberger G. Styrene synthesis in a reverse flow reactor. *Chem Eng Sci*. 1994;54:2637–2646.
18. De Groote AM, Froment GF. Synthesis gas production from natural gas in a fixed bed reactor with reversed flow. *Can J Chem Eng*. 1996;74:735–741.
19. Gosiewski K, Bartmann U, Moszczynski M, Mleczko L. Effect of the intraparticle mass transport limitations on temperature profiles and catalytic performance of the reverse-flow reactor for the partial oxidation of methane to synthesis gas. *Chem Eng Sci*. 1999;54: 4589–4595.
20. Gosiewski K. Simulations of non-stationary reactors for the catalytic conversion of methane to synthesis gas. *Chem Eng Sci*. 2001;56: 1501–1510.
21. Blanks RF, Wittrig TS, Petersen DA. Bidirectional adiabatic synthesis gas generator. *Chem Eng Sci*. 1990;45:2407–2413.
22. Neumann D, Kirchhoffb M, Veser G. Towards an efficient process for small-scale, decentralized conversion of methane to synthesis gas: combined reactor engineering and catalyst synthesis. *Catal Today*. 2004;98:565–574.
23. Neumann D, Veser G. Catalytic partial oxidation of methane in a high-temperature reverse-flow reactor. *AIChE J*. 2005;51:210–223.
24. Neumann D, Gepert V, Veser G. Some considerations on the design and operation of high-temperature catalytic reverse-flow reactors. *Ind Eng Chem Res*. 2004;43:4657–4667.
25. Simeone M, Salemme L, Scognamiglio D, Allouis C, Volpicelli G. Effect of water addition and stoichiometry variations on temperature profiles in an autothermal methane reforming with Ni catalyst. *Int J Hydrogen Energy*. 2008;33:1252–1261.
26. Grunwaldt JD, Hannemann S, Schroer CG, Baiker A. 2D-mapping of the catalyst structure inside a catalytic microreactor at work: partial oxidation of methane over Rh/Al_2O_3. *J Phys Chem*. 2006;110: 8674–8680.
27. Hannemann S, Grunwaldt JD, Vegten N, Baiker A, Boye P, Schroer CG. Distinct spatial changes of the catalyst structure inside a fixed-bed microreactor during the partial oxidation of methane over Rh/Al_2O_3. *Catal Today*. 2007;126:54–63.

Manuscript received Dec. 29, 2007, and revision received Apr. 7, 2008.